ELSEVIER

Physica A 298 (2001) 297–314

PHYSICA A

www.elsevier.com/locate/physa

Flow equations on a fractal structure

Marta González[a,b], Mariela Araujo[a,b,*], Adolfo Rodríguez[a]

[a] *Modeling and Reservoir Simulation Department, PDVSA Intevep, Caracas, Venezuela*
[b] *Escuela de Física, Facultad de Ciencias, Universidad Central de Venezuela, Venezuela*

Received 14 May 2001

Abstract

Two-phase flow equations are solved on a fractal Bernasconi lattice including capillary and viscous forces. The recursive structure of the lattice allows the use of a renormalization group approach to calculate flow properties, resulting in a much faster method compared to conventional simulations. The interplay between disorder or heterogeneity in local flow conductance and capillary pressure effects is studied as a function of length scale. Flow related quantities such as water cut curves, saturation profiles, and breakthrough times are found to depend on the size of the system and on disorder strength. As disorder increases larger sizes are needed to get good averaging. It is found that this lattice can be used to get a good approximated solution of the two-phase flow equations in complex anisotropic structures, since it grants considering the effect of anisotropy on flow properties, a condition relevant for a variety of industrial applications.

PACS: 47.55.M; 47.11; 47.53

Keywords: Two-phase flow; Bernasconi lattice; RG scheme; Anisotropy

1. Introduction

The understanding of the behavior of fluids inside a disordered structure is relevant to many industrial applications such as enhanced oil recovery, the efficient use of catalysts, the control of water pollution, and waste disposal among many areas [1–3]. The study is frequently done by solving the flow equations on an Euclidean lattice, or perhaps on a simple hierarchical structure properly selected for computational advantage [4]. There are situations however, where the disorder inherent to the structure is highly

* Corresponding author. EPMS. PDVSA Intevep, LTQ 1048, P.O. Box 8537, Miami, FL 33102, USA. Tel.: +58-21-29086077; fax: +58-21-29087781.
E-mail address: araujom@pdvsa.com (M. Araujo).

0378-4371/01/$ - see front matter
PII: S0378-4371(01)00274-6

complex, with a topology that cannot be easily mapped into a hypercubic or any other simple lattice. For those cases, it is convenient to use a fractal structure such as the Bernasconi lattice [5], which allows to model anisotropy effects commonly observed at large scales in real systems.

In this work, the Bernasconi lattice is used to solve two-phase flow equations for incompressible fluids including capillary and viscous forces. This lattice has been used previously by Hansen et al. [6] to handle two-phase flow using a real space renormalization group algorithm (RSR), when capillary forces are negligible. The numerical algorithm developed in this work also exploits the advantages of the recursive type of calculation of a RSR scheme, turning out to be about 40 times faster than conventional simulations performed on a hypercubic lattice. The computational savings achieved in our formalism allows to study the effect of disorder, anisotropy and scale on characteristic flow quantities such as saturation profiles, breakthrough times in displacement processes, and fluid recovery curves among others.

In a typical simulation of an oil reservoir or an aquifer, it is important to model the behavior of fluid flow at various scales [3,4]. Very frequently, the information available from laboratory tests is in the range of millimeters to centimeters, whereas the simulation cells used to model the reservoir may be larger than a few hundred meters or even a few kilometers. Thus, we are interested in the flow behavior at scales that differ in length factors of the order 10^6–10^8. Besides the role of the length scales, another important aspect is the fact that only statistical information can be gathered.

In general, there is a limitation on the size of simulation cells that may be used to model a reservoir. Each grid cell has effective property values defined according to the type of modeling that is relevant to the study. Since the available information is measured at a fine scale, the effective properties are assigned based on the requirement of similarity between the flow behavior at the small and the large scales. Aside from the limitation of the cell size, the numerical approach used in the simulation is also important [3,4]. In a conventional simulation, the solution of the flow equations on a hypercubic lattice require the use of matrices and the performance of matrix operations, such as inversion, which are known to be computationally very expensive.

Recent work [7–9] has shown the advantages of using hierarchical structures to solve flow equations. These advantages are given basically in terms of computer time and memory savings. However, these hierarchical lattices may have severe limitations when it is necessary to consider effects due to anisotropy heterogeneities, commonly observed in real systems, such as oil reservoirs and aquifers.

In this work, we present the structure used and the numerical formalism developed to solve the flow equations in Section 2. Then, results from two-phase flow simulations on the fractal lattice, and a comparison with similar experiments performed on a square lattice and a hierarchical structure with an eight shape appear in Section 3. Section 4 deals with anisotropy effects on flow properties, and finally a summary and conclusions are given in Section 5.

2. Model description and flow equations

A good understanding of the fluid behavior at any scale requires a detailed flow simulation to capture the effects of spatial heterogeneities, correlations, and anisotropy, which are normally ignored or poorly considered in usual average estimates. For this task, a numerical model is proposed. This model must guarantee that the solution of the flow equations for the given geometry, with particular initial and boundary conditions, represents the state of the system at a given time. The process normally leads to the development of a simulation program, which is used for the computation of a specific quantity or the determination of an effective property.

As a basic lattice we consider a recursive structure generated by the repeated application of the motif shown in Fig. 1. The motif is build using five bonds arranged in a Wheatstone bridge, as indicated in Fig. 1 as order 1 construction. For the next generation, each bond is replaced by the same motif, and the process is repeated up to the desired order.

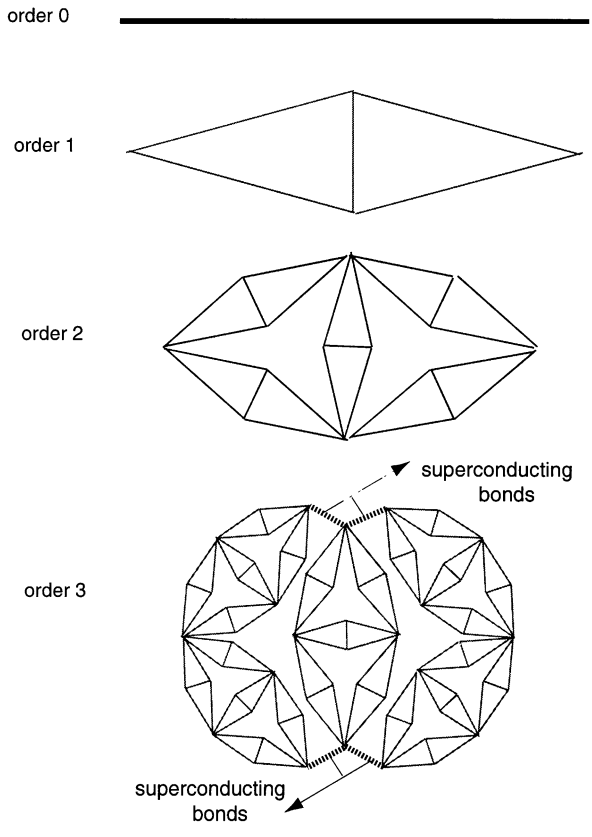

Fig. 1. Basic motif and recursive scheme for generation of the Bernasconi lattice.

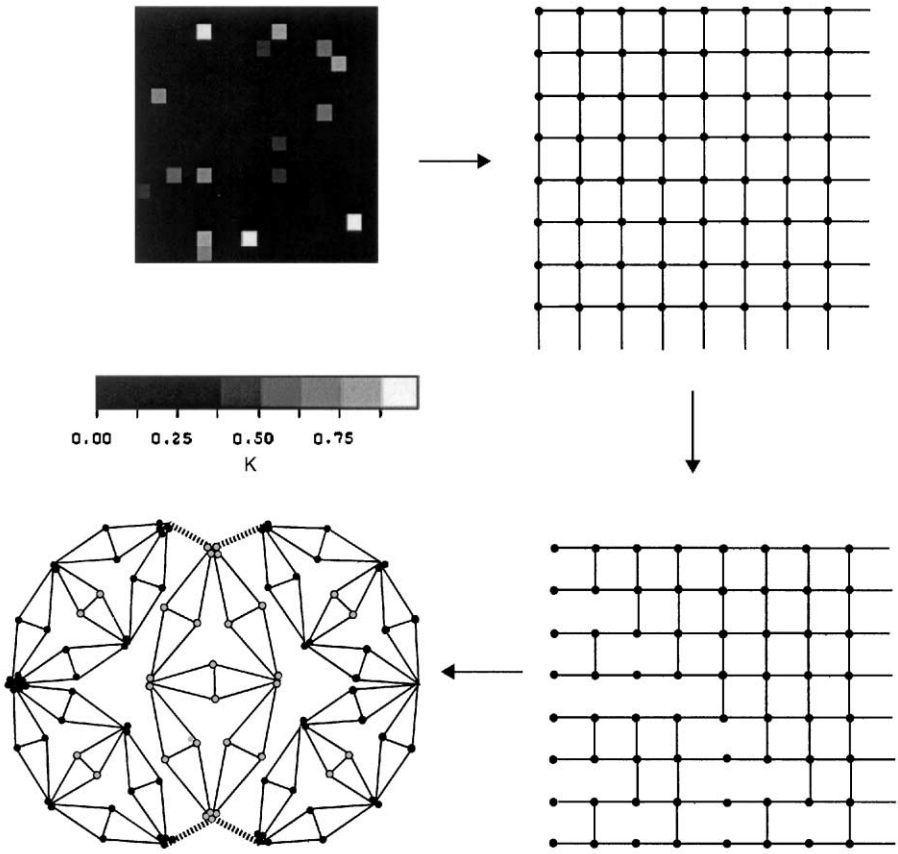

Fig. 2. Schematic representation of the assignment of local properties from a continuous medium to the fractal lattice.

Even though this lattice is generated in a two-dimensional space, it leads to a structure with a fractal dimension $d_F = \log 5/\log 2$. There are some bonds, here labeled as superconducting, that need to be together to assemble the structure. This is known as the Bernasconi lattice [5]. It was reported for first time in the calculation of effective conductances of random resistor networks, by using a renormalization group approach (RG).

In a typical situation, the formulation begins by describing a piece of disordered material that we want to study. Assuming that it can be considered as a continuous medium, it is discretized into cells as represented schematically in Fig. 2. To such a discretized system, we associate a square lattice whose vertical and horizontal bonds are chosen as indicated, forming an H-shaped structure in each case. These structures give rise to the fractal lattice.

To each bond of the lattice we assign local properties. One of the most relevant properties for fluid transport is the absolute permeability, which is a measure

of the flow conductance. Permeability values at the fine scale are taken from a power law-distribution of the form

$$g_{PL}(k) = |\mu| k^{\mu-1} . \tag{1}$$

Parameter μ is in the range $0 < \mu < 1$. It allows modeling a uniform permeability distribution when $\mu \to 1$, and a strongly disordered system where the permeability contrast may be as large as 30 orders of magnitude when $\mu \approx 0.1$. The advantage in using this type of distribution instead of others such as the lognormal, resides in the fact that by just changing one parameter, one can model weakly heterogeneous structures as well as extremely heterogeneous ones.

The approach used here consists essentially of two steps: (i) the transformation of the original lattice into a fractal (Bernasconi) lattice and (ii) the resolution of the flow equations including capillary forces on the recursive structure. In this way we take advantage of the self-similar property of the fractal structure, which allows getting an approximated solution at considerable reduced computer times when compared to conventional simulations.

On the structure, the following incompressible two-phase flow equations are solved:

$$S_w + S_n = 1 , \tag{2}$$

$$\phi \frac{\partial S_w}{\partial t} = -\nabla \cdot \vec{q}_w, \quad \phi \frac{\partial S_n}{\partial t} = -\nabla \cdot \vec{q}_n . \tag{3}$$

S_i are the saturation of the wetting (w) and non-wetting (n) phases, respectively, and ϕ the porosity of the sample. The phase flux is given by the generalization of Darcy's law [2]

$$\vec{q}_i = -\frac{k k_{ri}}{\mu_i} \nabla p_i , \tag{4}$$

where k is the absolute permeability, k_{ri} the relative permeability of phase i, μ_i the viscosity of phase i, and p_i the corresponding phase pressure. The difference in pressure of the non-wetting and wetting phase is known as the capillary pressure p_c. The permeabilities k_{ri} and the capillary pressure p_c are non-trivial functions of the phase saturation and the saturation history [2]. In this study, typical Brooks–Corey curves are used to model the saturation dependence of these quantities [10]. These are given by

$$k_{rw} = k_{rw}^o \left(\frac{S_w - S_{wi}}{1 - S_{or} - S_{wi}} \right)^{n_w} = k_{rw}^o (S_r)^{n_w} , \tag{5}$$

$$k_{rn} = k_{ro}^o (1 - S_r)^{n_n} , \tag{6}$$

$$p_c(S_r) = p_b (S_r)^{-1/\lambda} , \tag{7}$$

where S_{wi} and S_{nr} are the residual saturations of the wetting and non-wetting phases, respectively; n_w, n_n, and λ are the Corey exponents for the relative permeabilities and capillary pressure, quantities dependent in a non-trivial way on the pore geometry and

wetting affinity of the solid surface, and p_b is the entry pressure or the minimum pressure required to displace the wetting fluid.

The implicit pressure explicit saturation (IMPES) [4] scheme is used to solve the flow equations following an upwind criterion, in which the local relative permeabilities are weighted according to the local flow direction [3]. Since capillary pressure is taken into account, the total flux between any two nodes i and j consists of a viscous term and a capillary flux given by

$$Q_{ij} = g_{i,j}(p_{i,n} - p_{j,n}) - Q_{i,jc}\,, \tag{8}$$

where $g_{i,j}$ is the total conductance of the bond between nodes i and j for any of the fluids (one for the wetting phase and another for the non-wetting phase). The conductance of a bond to the wetting fluid is defined as

$$g_{i,jw} = \left(\frac{Ak_{ij}}{l\mu}\right) k_{rw}(S_w)\,, \tag{9}$$

A is the cross-sectional area and l the bond length. A similar expression holds for the conductance of the non-wetting phase. The total conductance is given by

$$g_{i,j} = g_{i,jw} + g_{i,jn}\,. \tag{10}$$

We assume that initially each node on the lattice has an initial saturation, and that all the nodes have the same porosity.

An unsteady state displacement simulation is performed on the structure, injecting the wetting fluid into a system with an initial saturation distribution composed mainly of the non-wetting fluid. The experiment may be done at a constant injection rate or constant gradient pressure across the sample. The injection itself is done on the left border of the lattice, with no flow conditions on the top and bottom boundaries.

The saturation of each node is updated by using Eq. (3), which is expressed as the difference between the fluid that enters the node and the fluid that flows out of the node by explicit integration

$$S_{iw}(t+\Delta t) = S_{iw} + \frac{\Delta t}{\varphi}\left(\sum_{i,in} Q_{i,inw}(t) - \sum Q_{i,outw}\right)\,. \tag{11}$$

In (11) φ is the pore volume, defined as a function of porosity as $\varphi = \phi Al$. The time step, Δt, is chosen such that the maximum wetting-phase saturation change at any time is 0.01.

It is important to note that in the mapping from the square lattice into the fractal lattice, one bond on the square lattice may have more than one bond associated in the fractal lattice. However, not all the bonds of the square lattice are used to construct the fractal lattice. This difference must be taken into account when doing comparisons with simulations performed on such lattices (here the square lattice and the hierarchical eight-shaped lattice).

Also, important in this context is the assignment of the pore volume since it depends on the bond assignment. The pore volume in the fractal lattice is assigned by summing

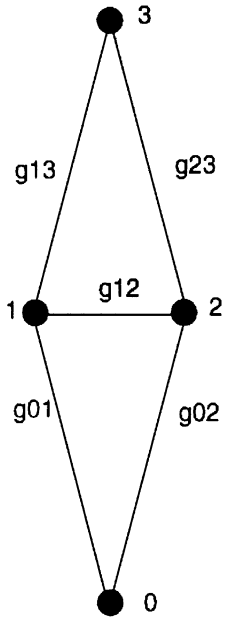

Fig. 3. Detail of lozenge or basic fractal lattice motif.

the volumes of all the bonds connected to a given node, and then multiplying it by a 1/3 factor, that is

$$\varphi_i = \frac{1}{3}\sum_j \varphi_{i,ij} \,, \tag{12}$$

with φ_i being the pore volume of node i on the fractal lattice, and $\varphi_{i,ij}$ the pore volume of the extreme of the ij bond. In the case of a homogeneous system, the central bond of the basic motif does not transport any flow and the fractal Bernasconi lattice reduces to a Berker or diamond lattice [11]. For this lattice the pore volume assignment has a weight factor of 1/2 instead of the 1/3 of Eq. (12).

The renormalization scheme is used to calculate the currents that flow along the bonds of the lattice. The main reason for using this renormalization method is that two-phase flow equations can be solved much faster than in the square lattice [12,13]. Assuming that for a given time the bonds shown in Fig. 3 have conductances g_{01}, g_{02}, g_{12}, g_{13} and g_{23}, respectively, and that there is a pressure difference P_{03} between nodes 0 and 3, the following system of equations must be solved in order to find the flow rates through each bond:

$$\frac{q_{01}}{g_{01}} + \frac{q_{13}}{g_{13}} = P_{03} \,, \tag{13}$$

$$\frac{q_{02}}{g_{02}} + \frac{q_{23}}{g_{23}} = P_{03} \,, \tag{14}$$

$$\frac{q_{01}}{g_{01}} + \frac{q_{12}}{g_{12}} - \frac{q_{02}}{g_{02}} = 0\,, \tag{15}$$

$$q_{12} + q_{13} - q_{01} = r_{Ic}\,, \tag{16}$$

$$q_{02} + q_{12} - q_{23} = r_{IIc}\,, \tag{17}$$

with $r_{Ic} \equiv q_{c_{12}} + q_{c_{13}} - q_{c_{01}}$ and $r_{IIc} \equiv q_{c_{02}} + q_{c_{12}} - q_{c_{23}}$, respectively. Here q_c depends on g_w and Δp_c. The solution of these equations give the flow rates at each bond: q_{01}, q_{02}, q_{12}, q_{13} and q_{23}, which depend on: P_{03}, g's, q_c's. From these values, we may find an expression for the total flow rate separating viscous and capillary effects

$$Q_{03} = G_{03}P_{03} - Q_{c03}\,, \tag{18}$$

where G_{03} is the effective conductance, and Q_{c03} takes account of the total capillary flux effect. It is easy to verify that

$$G_{03} = \frac{g_{02}d_{02} + g_{01}d_{01}}{r}\,, \tag{19}$$

$$Q_{c03} = \frac{q_{c01}d_{01} + q_{c02}d_{02} + q_{c12}d_{12} + q_{c13}d_{13} + q_{c23}d_{23}}{r}\,, \tag{20}$$

with

$$d_{01} \equiv g_{23}g_{13} + g_{02}g_{13} + g_{23}g_{12} + g_{13}g_{12}\,, \tag{21}$$

$$d_{02} \equiv g_{23}g_{13} + g_{23}g_{01} + g_{23}g_{12} + g_{13}g_{12}\,, \tag{22}$$

$$d_{12} \equiv -g_{02}g_{13} + g_{23}g_{01}\,, \tag{23}$$

$$d_{13} \equiv g_{12}g_{02} + g_{23}g_{01} + g_{01}g_{02} + g_{01}g_{12}\,, \tag{24}$$

$$d_{23} \equiv g_{02}g_{13} + g_{01}g_{02} + g_{01}g_{12} + g_{12}g_{02} \tag{25}$$

and

$$r \equiv g_{12}g_{02} + g_{02}g_{13} + g_{01}g_{02} + g_{23}g_{12} + g_{23}g_{13} + g_{23}g_{01} + g_{13}g_{12} + g_{01}g_{12}\,. \tag{26}$$

These expressions allow calculating the flow rates across each bond on a fractal lattice of any size through a recursion algorithm. Given values of g's for each bond and the p_c's for each node at the fine scale, G's and Q_c's can be calculated for a renormalized lattice. This process is repeated until effective values of G and Q_c are obtained for the entire lattice. Once the flow rates are known, the saturations can be updated (by explicit time integration) using Eq. (11). This method of calculation is more efficient than conventional ones in the sense that for a lattice of size $N = 4^{ord}$, we need $5^{ord} = N^{\log 5/\log 4} \approx N^{1.16}$ operations instead of the N^3 operations needed for solving the same equations on a square lattice.

3. Two-phase flow simulations: a displacement experiment

A displacement experiment is performed on the fractal lattice by injecting the wetting fluid on the left-hand side of the lattice, and measuring the fluid production on the right-hand side. The top and bottom boundaries have the conditions of no flow. Initially, each node has non-wetting-phase saturation of 0.80. The residual wetting-phase saturation is 0.25 and 0.2 for the non-wetting phase, respectively. The porosity of the sample is 0.3. In the simulation, the Brooks–Corey correlations are used with exponents $n_w = 4$, $n_n = 2$ and $\lambda = 2$, respectively.

3.1. Saturation profiles

In Fig. 4 a typical saturation profile after the injection of 0.25 pore volumes of wetting fluid in a system of order 5 is shown. The solid line corresponds to the profile obtained for a 1D homogeneous system. In the homogeneous system all the bond permeabilities have the same value, normalized to 1. The excellent agreement of both profiles is clearly seen.

When the capillary pressure is included, the profiles are smoother and the corresponding saturation decrease in value. This is expected from the fact that the capillary pressure term responds to saturation gradients on the sample. The excellent agreement between the profiles obtained for a 1D homogeneous system and the fractal lattice is observed in Figs. 5(a) and (b) for entry pressures of 1.5 and 3.0, respectively.

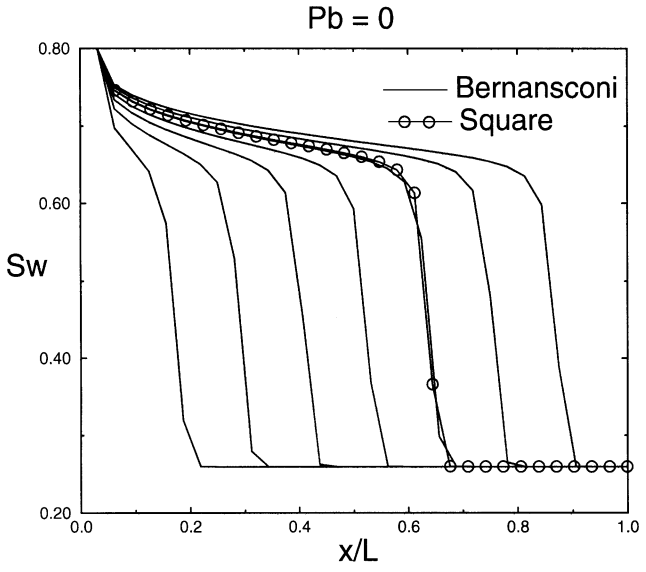

Fig. 4. Saturation profile after the injection of 0.25 pore volumes of wetting fluid into a homogeneous system without capillary pressure effects.

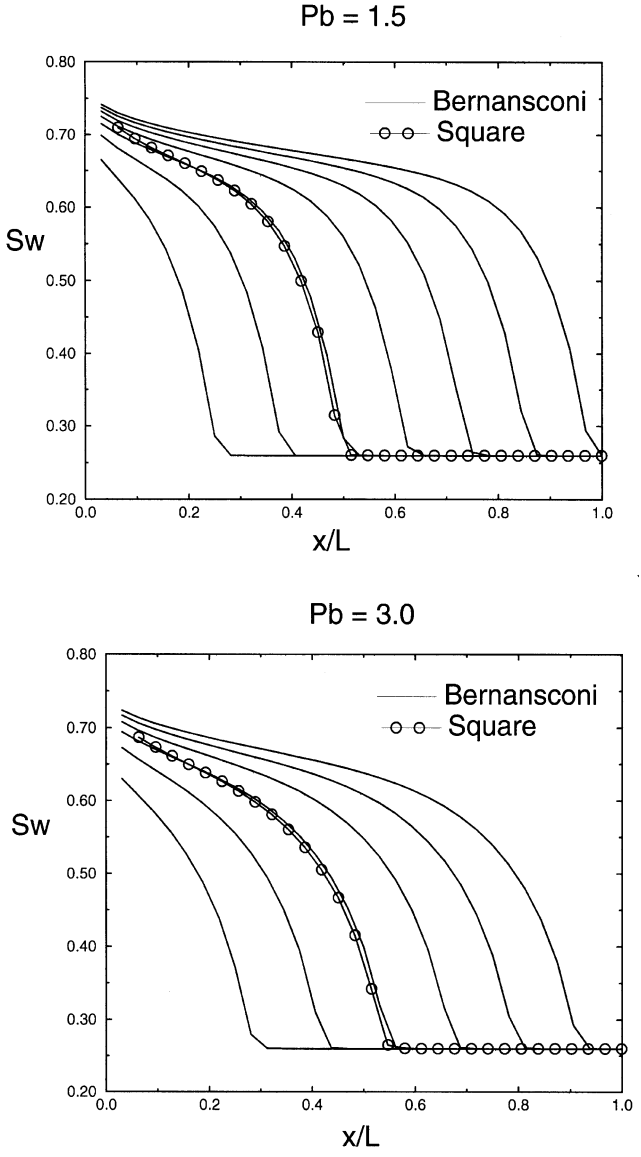

Fig. 5. Saturation profiles after the injection of 0.15 pore volumes of wetting fluid into a homogeneous system including capillary pressure effects. (a) Entry pressure $p_b = 1.5$ and (b) $p_b = 3.0$.

3.2. Saturation maps

Saturation maps for systems of size 32×32 and various disorder conditions are shown in Figs. 6 and 7. They correspond to the saturation values at the nodes of the fractal lattice mapped onto a square lattice for easier visualization. Fig. 6 corresponds

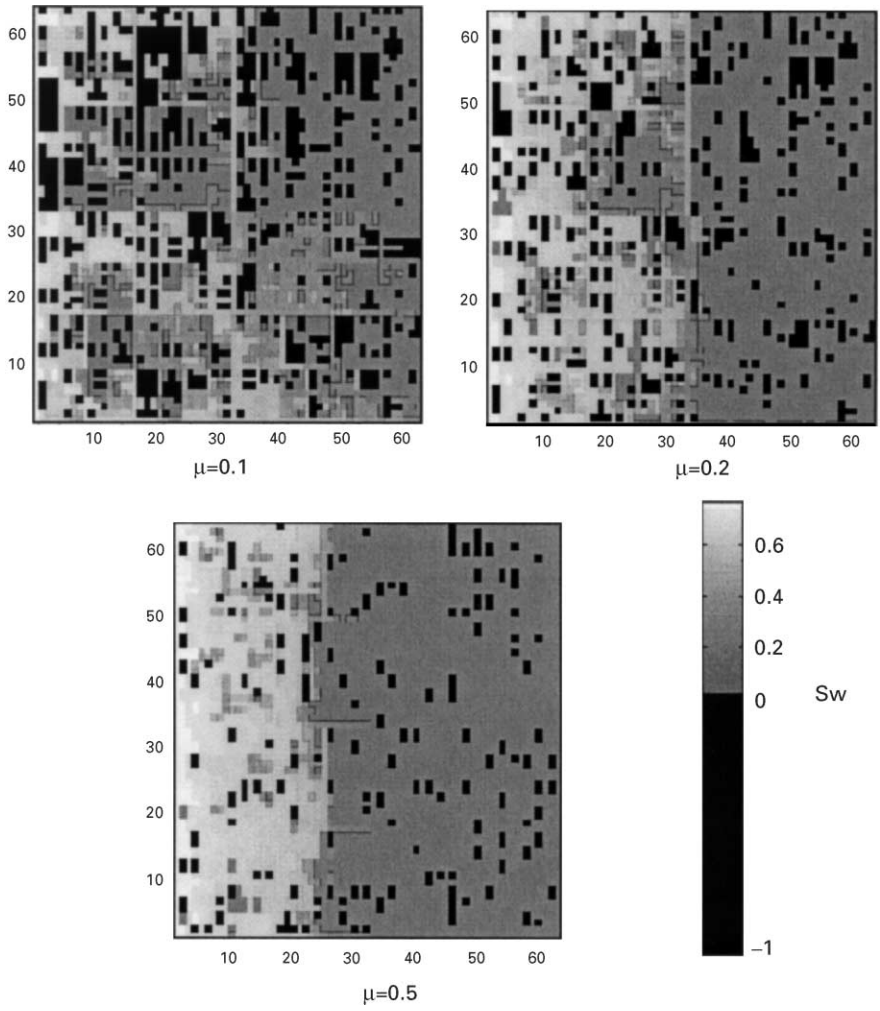

Fig. 6. Saturation maps after the injection of 0.15 pore volumes of wetting fluid into a fractal lattice for various disorder conditions without capillary pressure effects. The map represents a mapping of the nodes from the fractal lattice into a square lattice. Black sites denote blocked sites.

to the solution of the flow equations without the capillary pressure term, whose effect is represented explicitly in Fig. 7. A few observations about the maps are in order:

(i) In the figures, the black areas represent blocked sites. The term blocked site is used to describe those sites that were cut after the solution of the single-phase flow case (for having the smaller contribution to the flow) in order to get the same pore volume of an equivalent square lattice.

(ii) According to the gray scale used here, the initial condition was selected such that a uniform light gray extends over all the allowed nodes on the lattice. The injected wetting fluid is represented by white. It is seen from Fig. 6 that the best

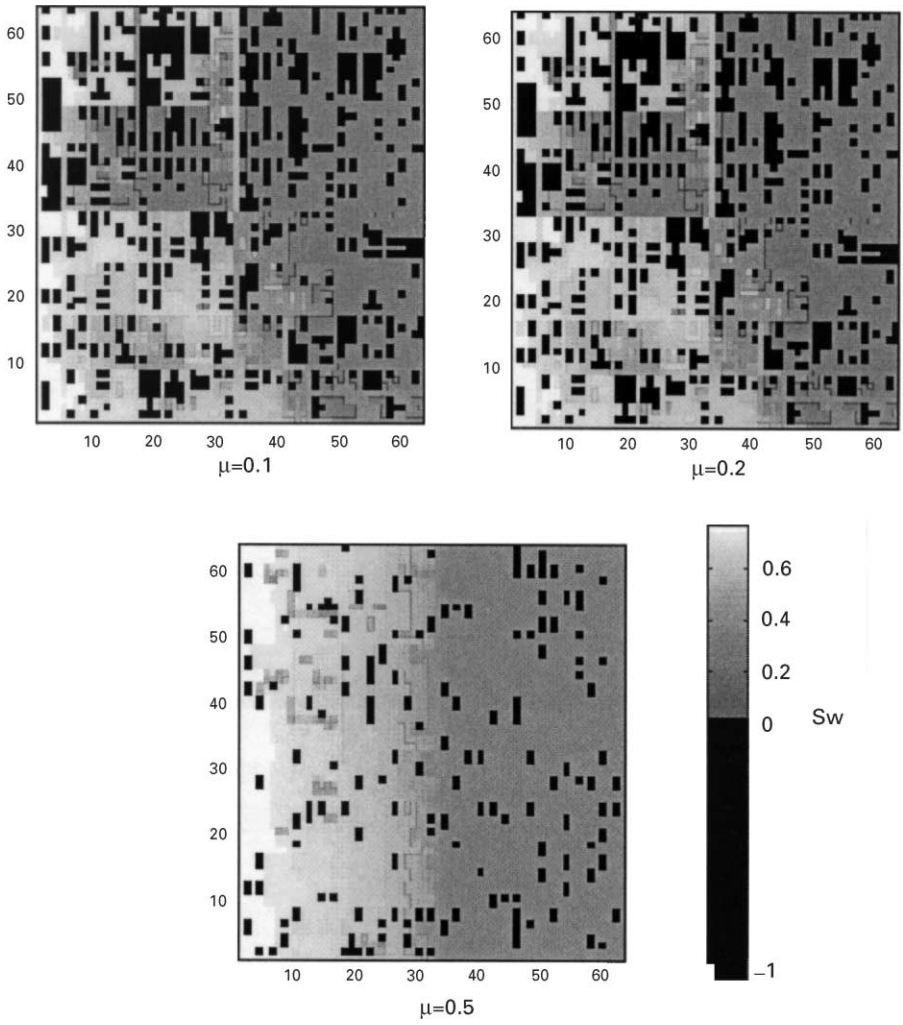

Fig. 7. Saturation maps after the injection of 0.15 pore volumes of wetting fluid into a fractal lattice for various disorder conditions with capillary pressure effects. The map represents a mapping of the nodes from the fractal lattice into a square lattice. Black sites denote blocked sites.

sweep efficiency is obtained for a homogeneous system or for a system with a mild disorder condition of $\mu = 0.5$.

(iii) When there is no capillary pressure effect, the front advance inside the lattice is rather sharp, leading to strong saturation gradients inside the sample.

(iv) With capillary pressure, these advancing fronts are smoothed out, and the saturation gradient inside the sample is much smaller (see Fig. 7).

(v) It is important to note that there are more nodes in the fractal lattice than in the square lattice, where the saturation information is being mapped. In the mapping

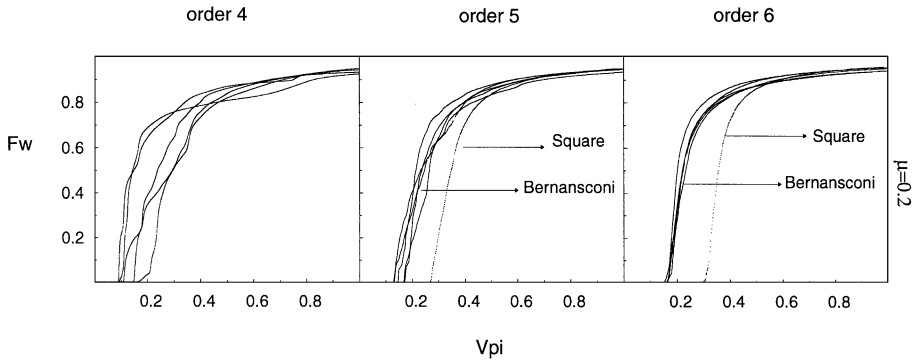

Fig. 8. Water cut curves as a function of size for a fractal system with disorder condition described by $\mu = 0.2$. The dotted line is the result from the solution of flow equations on a square lattice.

process an average of the node saturation is used to represent the different bin values.

3.3. Size and disorder effect on water cut curves

The effect of size on the water production curves, also known as water cut or irruption curves is summarized in Fig. 8 for a disorder condition of $\mu = 0.2$. Each square represents the production curves of five different experiments (small scale permeability values). The dotted line represents the corresponding curves obtained when solving the flow equations on a square lattice by using conventional methods. The difference in the breakthrough times is related to the different pore volume associated to each lattice. In order to make a quantitative comparison between the two lattices it is necessary to remove some bonds of the fractal lattice in order to have the same pore volume on both lattices. This bond cutting is performed based on the values of the bond currents after a single-phase flow run by removing the bonds that have the smaller currents.

Fig. 9 summarizes the effects of size and disorder for 10 different realizations of local permeabilities in a fractal lattice with the same pore volume as a square lattice. It is seen that for a given disorder condition (fixed μ value), the water production averages better as the system size increases. As disorder gets stronger (by decreasing the μ value) larger sizes are required to get the same good average. Also, it is observed that the breakthrough time is shorter for the more heterogeneous system, where the injected fluid experiences channeling, since more tortuous paths are followed due to the high permeability contrast existing in the sample. The breakthrough times on the fractal lattice are shorter than those obtained in a conventional 2D hypercubic lattice.

A comparison of the production curves obtained as a function of disorder and size is shown in Fig. 10 for the fractal lattice, a conventional 2D hierarchical lattice, and the eight-shaped lattice. We can understand the difference in the slope of the increase of the water production curve based on the number of allowed paths that the fluid

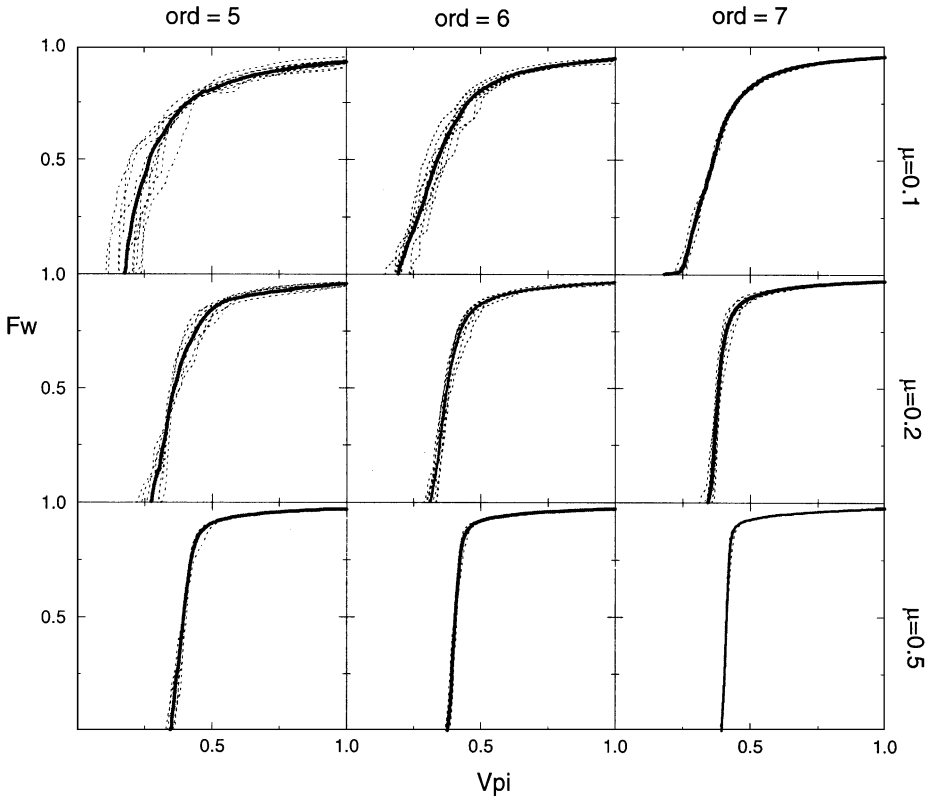

Fig. 9. Size and disorder effects of 10 realizations of local permeability on a fractal lattice with nodes removed to have the same pore volume as a square lattice. The solid line represents the average value.

must take to cross the sample. In the conventional square lattice the number is larger than those for the case of the eight-shaped lattice, and smaller than for the case of the fractal lattice, since we may have more paths that go across the larger number of nodes. Note the excellent agreement between the results obtained with the different structures.

3.4. Capillary pressure effects

In Fig. 11 the effects of the capillary pressure term on the water cut curves is shown. In a homogeneous system, it is seen that as the capillary pressure effect increases the breakthrough times are reduced in a way similar to the effect of the disorder on such lattice. The water cut curves are less steep as the p_b parameter in Eq. (7) gets larger.

When disorder is included, there is a competition between the disorder effect and the capillary pressure effect. It is seen that for a mild disorder condition described by $\mu = 0.5$, the capillary pressure effect is less pronounced when compared to a homogeneous system; however, the overall trend is similar on both systems. As disorder

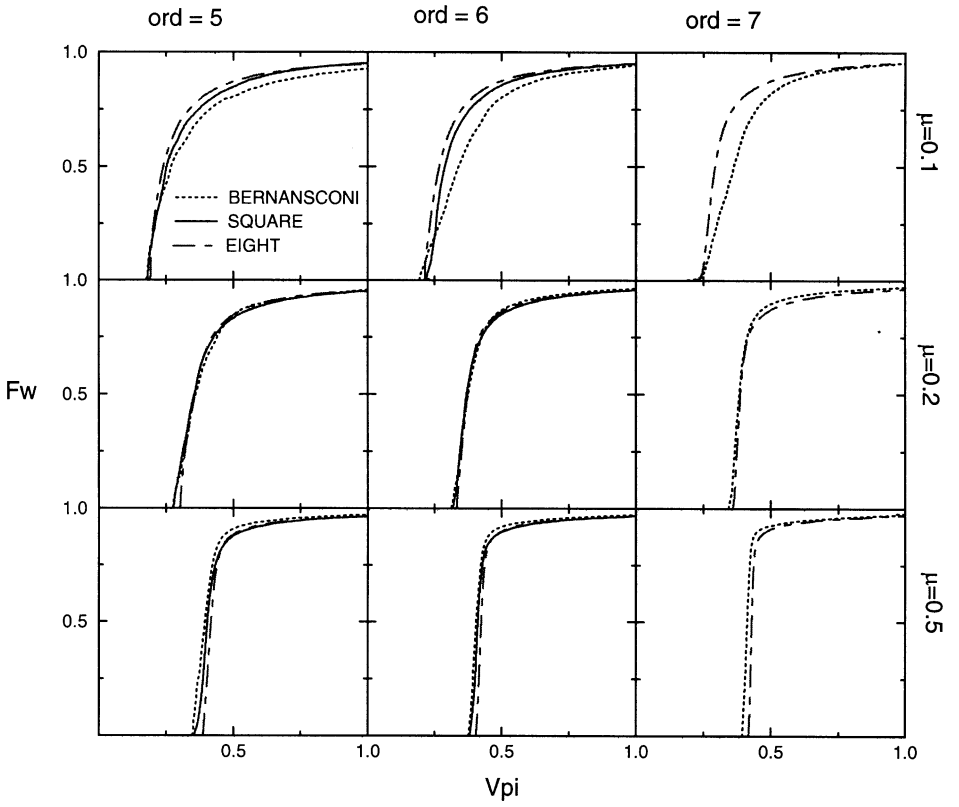

Fig. 10. Comparison of the effects of disorder and size on water cut curves on a fractal lattice, an eight-shaped hierarchical lattice and a square lattice.

is increased, it is observed that disorder effects become dominant over capillary ones. Now, the breakthrough times get larger when p_b increases, and the fastest breakthrough is observed when there are no capillary effects. In the figure, it is shown that when $\mu = 0.2$, both effects are of the same order, whereas for $\mu = 0.1$, disorder effects control the breakthrough time.

4. Anisotropy effects of flow properties

Oil reservoirs typically exhibit a significant permeability anisotropy. The knowledge of the impact of the anisotropy in fluid production has a significant economic importance in developing and managing such reservoirs, since it may help in the optimization of injection patterns to obtain the maximum sweep efficiency. Thus, it is interesting to study the impact of permeability anisotropy on the total recovery of a waterflood project, which is essentially the injection experiment that was referred to in the previous section [14].

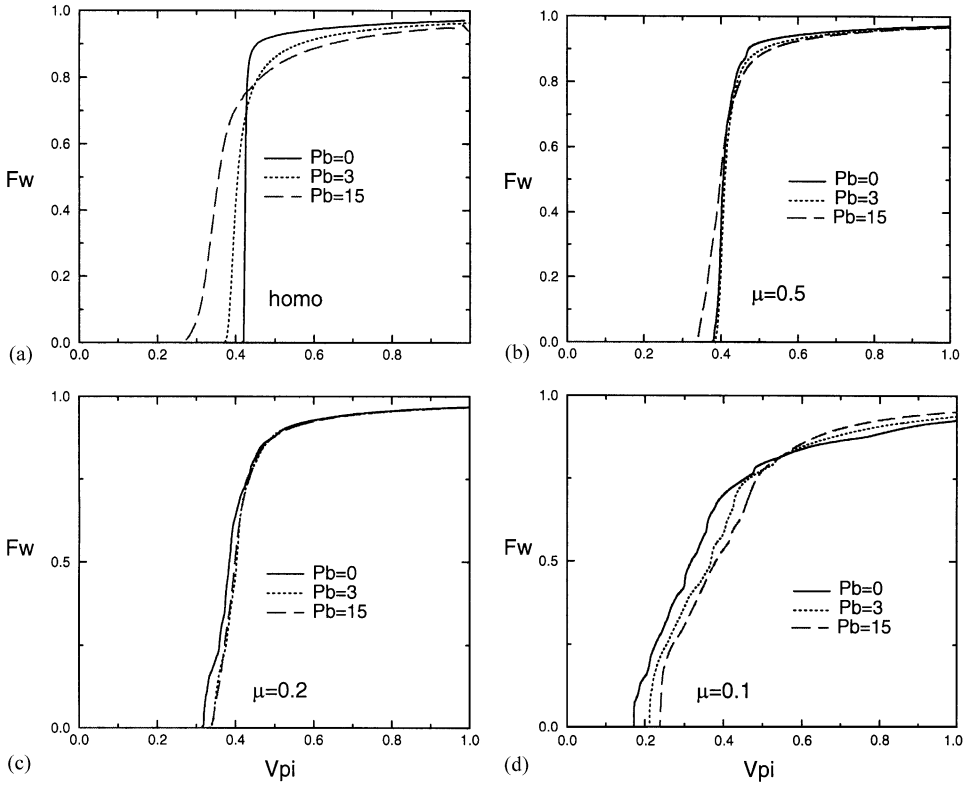

Fig. 11. Capillary pressure effects on the water cut curves for disordered systems of order 6.

The fractal Bernasconi lattice allows to investigate the effect of permeability anisotropy owing to the presence of the fifth bond on the basic motif structure of Fig. 1. The permeability anisotropy was varied altering the values of the horizontal and vertical transmissibilities of the gridblocks. To this end, we have run simulations on a lattice of order 5, with different permeability distributions assigned to the vertical and horizontal bonds of a corresponding square lattice mapping. The distributions are of power law form described by Eq. (1). The average and variance of this distribution is completely described by the μ parameter. Three cases that differ in an anisotropy ratio, defined as the ratio of the average value of the permeability of vertical bonds to the one of horizontal bonds, i.e., $\langle k_y\rangle/\langle k_x\rangle$ were compared: (a) an isotropic sample with $\langle k_y\rangle/\langle k_x\rangle = 1.0$ (the same μ parameter for the horizontal and vertical distribution), (b) an anisotropy condition with $\langle k_y\rangle/\langle k_x\rangle = 4.5$, and (c) an anisotropic situation with $\langle k_y\rangle/\langle k_x\rangle = 0.2$.

The same simulations were run on the Bernasconi fractal lattice with the method proposed in this work, and on a square lattice following conventional methods. The water production curves are given in Fig. 12 for the three anisotropy ratio and disorder condition described by $\mu = 0.2$. The same behavior is observed for $\mu = 0.5$ and 0.1,

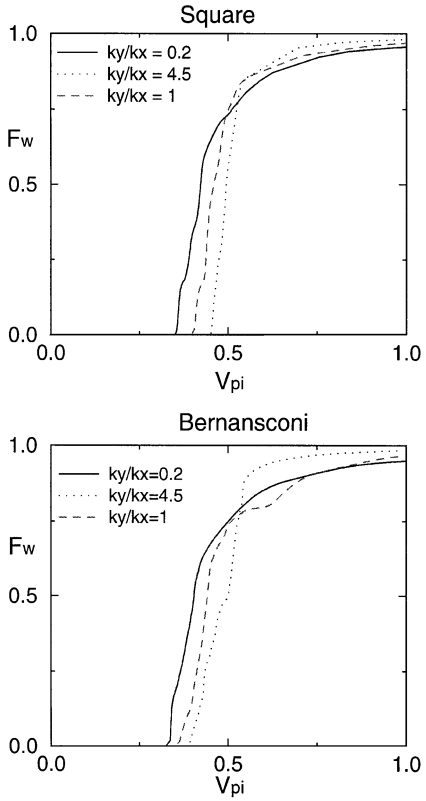

Fig. 12. Anisotropy effects on water cut curves for disordered systems of order 5 on the fractal and the square lattice. We compare the isotropic case with anisotropy ratio of 0.2 and 4.5, respectively.

respectively. As mentioned in Section 3, these μ values may be associated to mild, medium and strong disorder conditions.

A systematic trend is observed for all the cases. For an anisotropy ratio smaller than one (of 0.2 in Fig. 12), the breakthrough times are shorter than the values observed for an isotropic system, whereas for an anisotropy ratio larger than 1 (of 4.5 in Fig. 12), the breakthrough times are delayed with respect to the isotropic condition. The behavior of the breakthrough time with anisotropy can be understood in terms of the number of allowed paths that the fluid has in a particular case. For an anisotropy ratio smaller than 1, the vertical permeabilities are much smaller than the horizontal values, producing a sort of channeling behavior, and thus a smaller breakthrough time. On the contrary, when the anisotropy ratio is larger than 1, the vertical permeabilites are the ones that favor the fluid conduction. Since in the injection design the produced fluid is measured from the right-hand side of the sample, the fluid needs to go through longer paths giving rise to a later breakthrough time.

A similar study was done by Chang and Mohanty using conventional simulations [15].

5. Summary and discussion

We may summarize the main results presented here as follows:

A fractal lattice can be used to solve the two-phase flow equations including capillary pressure by using a renormalization group approach, which turns out to be at least 40 times faster than conventional simulation methods. These computational advantages allow to study the effect of size, disorder and anisotropy on flow properties including capillary effects. For a given system size, it is observed an interplay between capillary pressure and disorder effect which manifests on the breakthrough times behavior, making the interpretation of the fluid production curves a non-trivial one when both effects are present.

Acknowledgements

The authors thank PDVSA Intevep for permission to publish this paper.

References

[1] M. Sahimi, Rev. Mod. Phys. 65 (1993) 1393.
[2] J. Bear, Dynamics of Fluids in Porous Media, Dover Editions, New York, 1988.
[3] R. Helming, Multiphase Flow and Transport Processes in the Subsurface, Springer, Berlin, 1997.
[4] K. Aziz, A. Settari, Petroleum Reservoir Simulation, Applied Science Publishers, London, 1979.
[5] J. Bernasconi, Phys. Rev. B 18 (1978) 18.
[6] A. Hansen, S. Roux, A. Aharony, J. Feder, T. Jossang, H.H. Hardy, Transp. Porous Media 29 (1997) 247.
[7] R. Angulo, E. Medina, J. Stat. Phys. 75 (1994) 135.
[8] A.A. Rodríguez, M. Araujo, preprint 2000.
[9] A.A. Rodríguez, M. Araujo, SPE Paper 66390, 2001.
[10] R. Brooks, A. Corey, Proc. Am. Soc. Civil Eng. J. 92 (1966) 61.
[11] R.J. Creswick, H.A. Farach, C.P. Poole Jr., Introduction to Renormalization Groups Methods in Physics, Wiley Inter Science, New York, 1992.
[12] R.P. King, Transp. Porous Media 4 (1989) 37.
[13] R.P. King, A.H. Miggeridge, W.G. Price, Transp. Porous Media 12 (1993) 237.
[14] J.M. Wade, E.V. Hough, S.H. Pedersen, SPE Paper 48961, 1998.
[15] Y.C. Chang, K.K. Mohanty, J. Pet. Sci. Eng. 18 (1997) 21.